AIAA JOURNAL
Vol. 35, No. 6, June 1997

Direct Numerical Simulations of Wake Vortices in Intense Homogeneous Turbulence

Frédéric Risso* and Alexandre Corjon†
Centre Européen de Recherche et Formation Avancée en Calcul Scientifique, 31057 Toulouse Cedex, France
and
Alain Stoessel‡
Institut Français du Petrole, 92506 Rueil-Malmaison, France

Three-dimensional direct numerical simulations of a vortex pair placed in an homogeneous turbulent field are presented. The phenomenon of interaction between the vortices and the turbulence is analyzed in detail from two simulations calculated on a 135^3 nodes mesh grid (one case with axial core velocity, the other without). The results show that the role of large and small turbulent eddies can be separated into two fairly independent mechanisms. The large structures are stretched by velocity gradients induced by the vortex pair. That leads to the formation of both tubes of vorticity spinning azimuthally around each vortex and associated axial velocity sheets. These structures cause a strong decrease of the maximal velocity and the curvature of the vortices. These deformations induced by the turbulence initiate an antisymmetric long-wave instability of the pair, which will probably lead to the collapse of the vortices. Concurrently, the small structures can enhance the diffusion of the vorticity out of the vortex core. From this analysis and scale considerations, the correct form for a model of decay of the vortices is derived. On the other hand, nine simulations on a 81^3 nodes mesh grid are used to determine the sensibility of the results to the random turbulent initial conditions.

Nomenclature

a	= sound celerity
d_0	= spacing between vortices at t equals 0
E	= energy spectral density
F	= enstrophy
K_e, K_d	= wave numbers: energy and dissipation
k	= kinetic energy of turbulence
L	= size of the computational domain
P	= pressure
q	= coefficient of q vortex
Re	= Reynolds number
Re_Γ	= circulation-based Reynolds number
r	= distance from vortex center
r, θ, z	= cylindrical coordinate
r_c	= core radius
r_0	= initial core radius
t	= time
U_θ	= azimuthal velocity
$u\prime$	= rms velocity, m/s
$V_{\max}$	= maximal azimuthal velocity
V_0	= $V_{\max}$ at t equals 0
$W_{\max}$	= maximal axial velocity
x, y, z	= Cartesian coordinates
Γ	= circulation of individual vortex
Γ_0	= initial circulation
$\delta_{x,i}$, $\delta_{y,i}$	= magnitude of vortex deformation
ϵ	= turbulence dissipation rate
Λ	= integral length of turbulence
ν	= kinematic viscosity
ρ	= density
Φ_{ij}	= enstrophy tensor
Ω	= vorticity
$*$	= normalized quantities

Received Sept. 28, 1995; presented as Paper 96-0802 at the AIAA 34th Aerospace Sciences Meeting, Reno, NV, Jan. 15–18, 1996; revision received Oct. 8, 1996; accepted for publication Feb. 19, 1997. Copyright © 1997 by the American Institute of Aeronautics and Astronautics, Inc. All rights reserved.

*Researcher, Computational Fluid Dynamics Project; currently Researcher, Centre National de la Recherche Scientifique, Institut de Mécanique des Fluides de Toulouse, av. C. Soula, 31400 Toulouse, France.

†Senior Researcher, Computational Fluid Dynamics Project, 42, av. G. Coriolis. Member AIAA.

‡Research Engineer, Computer Science Department, 1-4 av. de Bois Préau. Member AIAA.

I. Introduction

A. General Context

THE first problems due to wake vortices appeared around 1970 with the arrival of very large aircraft such as the Boeing 747. Many fatal accidents occurred to smaller aircraft flying in the wake vortices of these large planes. The first study program was launched by the Federal Aviation Administration between 1969 and 1970 to solve this problem. An extensive data collection effort led to the definition of aircraft separation standards edited by the International Civil Aviation Organization and applied by many countries: a 3×3 matrix based on the maximum takeoff weight of the aircraft. The objective is to ensure safety by avoiding any encounter between wake vortices and a following aircraft. Unfortunately, with the constant traffic growth, these standards contributed to airport congestion. Subsequent studies tried to recover some of the airport capacity lost by optimizing the separation times but with the same level of safety. The operational efficiency of a new categorization depends on a better knowledge that the effects of meteorological conditions have on the lifetime and decay of wake vortices.

B. Wake Vortex Phenomenon

The main external factors affecting wake vortex decay are turbulence, stratification, ground effect, and wind. These factors have several effects on the stability, decay, and trajectories (rebound) of the vortices. In the following section, we will begin with a review of the literature of the turbulence effect.

1. *Stability*

The main mechanisms of instability are the bursting (for an isolated vortex) and the reconnection (for a vortex pair), which are initiated by the turbulence. The initial work on the trailing vortices instability is due to Crow[1] and Crow and Bate.[2] Crow[1] has defined the linking time of a vortex pair as a function of the turbulent dissipation rate. These theoretical works were confirmed by many experimental studies in towing tanks in a neutral medium,[3,4] or in a stratified fluid,[3] or even in the atmosphere.[5] The results of Sarpkaya and Daly[3] have shown that the Crow formula[1] is not valid for high

Reynolds numbers where the breakdown of the vortices is essentially due to the bursting phenomenon. Moreover, the reconnection of the vortices does not imply safe flying conditions for following aircraft. Some recent stability studies divide the effects due to short and long wavelength instabilities[6,7] and find that the Crow theory is an application case of a more general theory. They show that a vortex pair is always unstable when their circulation ratio is negative. The bursting phenomenon is not yet well understood. Vortex reconnection implies bursting but bursting does not lead to vortex reconnection. The work done on this subject focuses on the stability of one isolated vortex.[8–10]

The dramatic increase in computer speeds and the improvement of the numerical schemes permit researchers to study these complex phenomena by the use of direct numerical simulation (DNS). For example, the vortex pair reconnection is studied by Virk et al.[11] in the framework of fundamental turbulence studies but the results could apply to wake vortices. Another application of DNS for trailing vortices is presented by Spalart and Wray.[12] They give new insights on the Crow instability[1] initiated by the atmospheric turbulence and the operational interest of these results.

2. Decay Due to Turbulence

The second effect of the turbulence is to accelerate the vortex decay. Donaldson and Bilanin[13] proposed a model of diffusion for the aging of a vortex pair in the atmospheric turbulence. Their model depends on the aircraft wingspan and the rms velocity of turbulence [Eq. (15)]. These theoretical results are based on experimental results and scale analysis. Bilanin et al.[14] pursue this work by some numerical simulations with a Reynolds averaged Navier–Stokes solver. Robins and Delisi[15] and Zheng and Ash[16] perform similar two-dimensional studies for three cases: constant turbulent bath, mean crosswind shear, and ground effect. But until now, no improvement to the model proposed by Donaldson and Bilanin[13] in 1975 was obtained.

The work done by Squire[17] is also often used. The effect of turbulence is modeled with an equivalent eddy viscosity proportional to the circulation of an ideal laminar vortex. Owen[18] proposed an extension to this theory, and both these theories were experimentally studied by Iversen.[19] Other works, such as Philipps,[20] have found the relaminarization of the vortex core. More recently, Zeman[21] has shown that the evolution of the core radius is locally controlled by viscous effects as in the laminar case.

C. Present Work

Here, as in preliminary studies,[22,23] DNSs have been used to study the complex interaction between turbulence and wake vortices. First, the numerical tool and the simulations (Sec. II) are described. Then the results (Sec. III) are presented and discussed. The initiation of the Crow instability[1] is exhibited. But the main results concern the turbulent vortex decay for which a new model is proposed. Moreover, the conclusions are reinforced by a statistical analysis.

II. Presentation of the Simulations

A. Numerical Tool

The present NTMIX3D code[24] solves three-dimensional unsteady compressible Navier–Stokes equations. A highly accurate finite difference method over a Cartesian grid is used to fully handle most of the different scales in the three-dimensional flow: spatial derivatives are computed with a sixth-order compact scheme (Padé scheme),[25] which has the property of being low dispersive and nondissipative. These schemes allow some quasi-spectral accuracy. Time advancement is achieved with a third-order Runge–Kutta method.

The cost in CPU and memory of a three-dimensional simulation is so high that it requires the use of parallel computers to be affordable. Thus, the code has been written in parallel with a message passing paradigm. Specific domain decomposition methods have been developed for the parallel treatment of compact schemes[26] that allow the availability of a highly efficient version of the code on a wide range of distributed memory parallel computers such as IBM SP2, Fujitsu VPP500, and Cray T3D. For instance, on a Fujitsu VPP500 with 18 nodes, a 210^3 grid is handled in less than 200 Mwords of memory and with a cost of 0.33 μs/gridpoint/timestep. The simulations presented in the following have been run on a VPP, a Meiko CS2, or a Cray T3D.

B. Initial Conditions

All of the simulations presented here have been performed on a regular grid. The initial conditions have been built by the superimposition of the two flowfields induced by a vortex pair and an homogeneous isotropic turbulence. Then, the time evolution of the whole flowfield has been calculated by solving the full compressible Navier–Stokes set of equations in a periodic domain.

1. Vortex Pair

For the initial conditions, we have used analytic expressions for the vortices. The Lamb–Oseen vortex was chosen: an unsteady solution of the Navier–Stokes equations for the evolution of an initial line vortex characterized by a circulation Γ (see Ref. 27). It effectively models the vortices shed by an aircraft: quasisolid rotation into the core and constant circulation at the infinity. If the cylindrical coordinates (r, θ, z) are considered, the induced velocity $\boldsymbol{U}$ is only azimuthal and depends only on r:

$$\frac{U_\theta(r)}{V_{\max}} = \alpha\frac{r_c}{r}\left\{1 - \exp\left[-\beta\left(\frac{r}{r_c}\right)^2\right]\right\} \tag{1}$$

The magnitude of the velocity circulation, which could be obtained from the integration of Eq. (1), does not decrease anywhere, thus the criterion of Rayleigh[8] is satisfied and stability is ensured. The pressure P is given by the integration of

$$\frac{\mathrm{d}P}{\mathrm{d}r} = \rho\frac{U_\theta^2}{r} \tag{2}$$

The spatial structure of the Lamb–Oseen vortex is a function of two parameters: the maximal azimuthal velocity $V_{\max}$ and the core radius $r_c[U_\theta(r_c) = V_{\max}]$. The two constants α and β are solutions of the following equations:

$$1 + 2\beta = \exp(\beta) \Rightarrow \beta \simeq 1.2544 \tag{3}$$

$$\alpha = \frac{1}{1 - \exp(-\beta)} \Rightarrow \alpha \simeq 1.40 \tag{4}$$

In the theoretical laminar solution, the time evolution does not modify the velocity distribution given by Eq. (1). Consequently, the conservation of the kinetic momentum imposes that the circulation at infinity remains equal to the initial value Γ. The aging of the vortex can be expressed by the evolution of r_c and $V_{\max}$, which depends on the kinematic viscosity ν,

$$r_c(t) = \sqrt{4\beta\nu t} \tag{5}$$

$$V_{\max}(t) = \frac{\Gamma}{2\pi\alpha r_c} = \frac{\Gamma}{2\pi\alpha\sqrt{4\beta\nu t}} \tag{6}$$

For the Lamb–Oseen vortex, the maximal value of the vorticity magnitude $\Omega_{\max}$ varies as the inverse of time:

$$\Omega_{\max}(t) = \frac{2\alpha\beta V_{\max}(t)}{r_c(t)} = \frac{\Gamma}{4\pi\nu t} \tag{7}$$

As shown by Batchelor,[28] the process of formation of the wake vortices leads to the existence of an axial velocity in the core region. Lessen and Paillet[9] introduced the q vortex by approximating the axial velocity by a Gaussian law,

$$\frac{U_z(r)}{W_{\max}} = \exp\left[-\beta\left(\frac{r}{r_c}\right)^2\right] \tag{8}$$

with

$$W_{\max} = (\alpha\sqrt{\beta}/q)V_{\max}$$

In the present work, the simulations referred to as G_1, P_1–P_9, and P_{lam} (see Table 1) used the Lamb–Oseen type vortex [Eq. (1)] without axial velocity. For the case G_2, the q vortex was chosen [Eqs. (1) and (8)]. In all cases, no initial radial velocity was present, and the flowfield was homogeneous in the axial direction. The pressure field

Table 1 Characteristics of the simulations

Cases	Mesh grid	Domain size $L*$	Re	$u/*$, $\epsilon*$, $\Lambda*$, $Re_T = \Lambda u/\nu$	$Ke*$, $Kd*$	Remarks
G_1	$135\times135\times135$	46.9	600	0.108, 4.7 10^{-5}, 2.85, 185	0.45, 4.5	Lamb–Oseen
G_2	$135\times135\times135$	46.9	600	0.108, 4.7 10^{-5}, 2.85, 185	0.45, 4.5	q-vortex ($W_0/V_0 = 1$) (initial turbulence like G_1)
P_{1_9}	$81\times81\times81$	28	600	0.108, 4.7 10^{-5}, 2.85, 185	0.45, 4.5	Lamb–Oseen (nine different initial turbulences)
P_{lam}	$81\times81\times81$	28	600	Undefined		Lamb–Oseen 2D (laminar case)
P_{thi}	$81\times81\times81$	28		0.108, 4.7 10^{-5}, 2.85, 185	0.45, 4.5	Without vortex (initial turbulence like P_9)

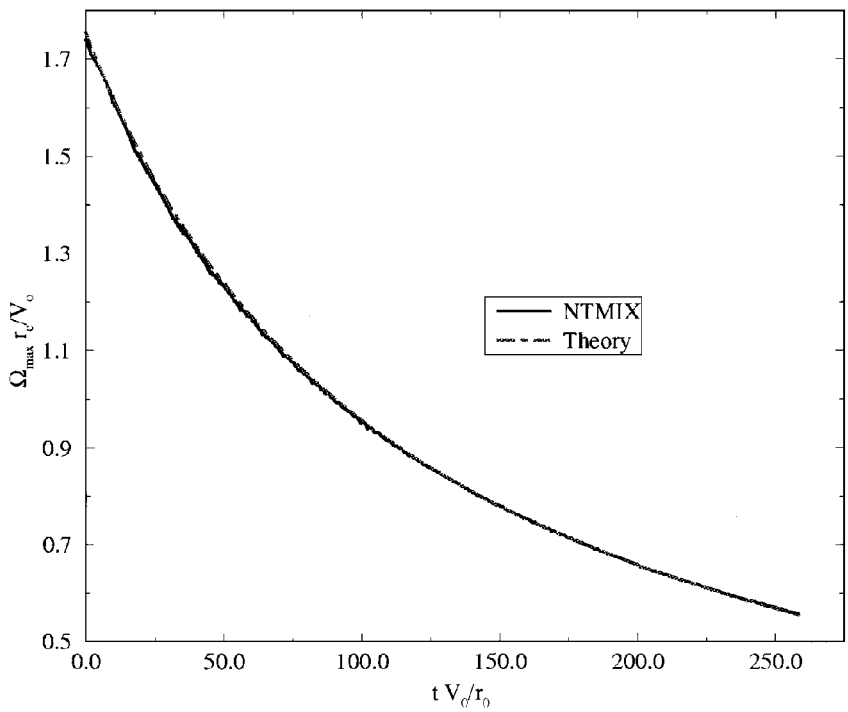

Fig. 1 Comparison of maximal vorticity decay with analytical law.

corresponding to each vortex was computed by integrating Eq. (2) considering the fluid at rest at infinity. The vortex pair consisted in two vortices parallel to the z axis with a spacing d_0 in the x direction. The flowfield of a pair is obtained by the linear superimposition of the velocity and pressure fields induced by each vortex, this superimposition being valid until the distance d_0 is equal to several core radii.

For the cases without axial velocity, the initial vortex pair is entirely defined by the following three dimensionless parameters:

$$Re = V_0 r_0/\nu = 600 = \Gamma/2\pi\alpha\nu = (1/2\pi\alpha)\, Re_\Gamma$$

$$d_0* = d_0/r_0 = 8$$

$$Ma = V_0/a = 0.2$$

The Reynolds number is small in comparison with the real phenomenon (by about four orders of magnitude). The spacing chosen is a typical value observed behind the aircraft.[29] The Mach number is sufficiently small for the compressible effects to be neglected. In the following, all quantities marked with an asterisk are normalized using the reference scales built on V_0 and r_0.

For the case G_2, the magnitude of the initial maximal axial velocity appearing in Eq. (8) also has to be fixed. Lessen and Paillet[9] have studied the stability of an isolated q vortex. Their results shows that the flow is stable for all modes of perturbations until $q > 1.5$, which has been confirmed by the study of Mayer and Powell.[30] To emphasize the difference for the case without axial velocity, we chose a value of the initial axial velocity close to the upper limit allowed by the criterion of stability,

$$W_0* = W_0/V_0 = 1.0 \Longrightarrow q \approx 1.57$$

To check the accuracy of our computations, we compared the analytical law for the decay of $\Omega_{\max}$ [Eq. (7)] and the result of NTMIX3D in the case P_{lam}. Figure 1 shows good agreement between the two cases and the accuracy of our computations.

2. Ambient Turbulence

The turbulence flowfield is initialized considering an isotropic homogeneous turbulence. This field is built in the spectral plane from a given spectrum with random phases for each mode. The formulation derived from the spectrum of von Kármán and Pao[31] is used for the energy spectrum $E(k)$,

$$E(K) = \frac{2}{3}\frac{3}{2}\frac{k^{\frac{5}{2}}}{\epsilon}\frac{(K/K_e)^4}{\left[1+(K/K_e)^2\right]^{\frac{17}{6}}}\exp\left[-\frac{9}{4}\left(\frac{K}{K_d}\right)^{\frac{4}{3}}\right] \qquad (9)$$

where K_e is the peak wave number of the energy spectrum and K_d one of the dissipation spectrum. The turbulence characteristics in the atmospheric boundary layer are described by Donaldson and Bilanin.[13] They proposed an approximate relation for Λ

$$\begin{aligned} \Lambda &= 1.3y \quad \text{for} \quad y \leq 169\ \text{m} \\ \Lambda &= 220 \quad \text{for} \quad y > 169\ \text{m} \end{aligned} \qquad (10)$$

In the numerical simulations, the value of the maximum length scale for turbulent eddies was limited by the computational domain size L. Here two domain sizes were used. In the simulations referred to as G_1 and G_2, the side length of the cubic domain was $L* = 46.9$ on a 135^3 nodes grid. In all other simulations, it was $L* = 28$ on a 81^3 nodes grid. To simulate the similar turbulence fields in all cases,

the mesh size was the same: $\Delta x* = \Delta y* = \Delta z* = 0.35$ and the minimal value of L was used to determine K_e from the following criterion:

$$2\pi/K_e \leq \tfrac{1}{2}L = 14r_c \tag{11}$$

Thus, we retained $2\pi/K_e* = 14$, which implied for the given spectrum (9) an integral scale $\Lambda* = 2.87$. Because the core radius behind a typical aircraft is between 1 and 3 m, this value is less than those observed in real atmospheric turbulence. Nevertheless, it ensures that the length scale characteristic of the most energetic eddies ($2\pi/K_e* = 14$) is larger than the vortex spacing ($d_0* = 8$). As we will see later, this point is of major importance in simulating the real situation. Considering measurements of atmospheric turbulence presented by Donaldson and Bilanin,[13] one notices that in the case of strong turbulence, the rms velocity of the turbulent fluctuation is about 10% of the maximal velocity induced by a vortex. For all present simulations we put $\sqrt{(2k)} = 0.108V_0$, which leads for the given spectrum to a dissipation of $\epsilon = 4.710^{-5}V_0^3 r_0^{-1}$ and to a size of the eddies corresponding to the peak in the dissipation spectrum four times larger than the resolution ($2\pi/K_d = 4\Delta x$). The present Crow's parameter[1] is $\eta = 0.412$ and corresponds to strong atmospheric turbulence observed during a flight test by Tombach.[5]

The turbulence field generated at $t = 0$ is not artificially maintained during the computation, and its intensity will decay with time. To study the effect of this decay, it is possible to compare the time scale of the turbulence and the time scale of the vortices. A characteristic time for the turbulence is the eddy turnover time T_t defined by the ratio of the integral length scale to the rms velocity. The corresponding characteristic time for the vortices, T_V, could be similarly defined by the ratio of the core radius to the maximal velocity. The comparison of these two characteristics times gives

$$\frac{T_t}{T_V} = \frac{\Lambda V_0}{r_0\sqrt{2k}} \simeq 26 \tag{12}$$

Turbulence decay is sufficiently slow compared to the vortex dynamics to obtain the main characteristics of the effects of the atmospheric turbulence on the wake vortices.

III. Results and Discussion

A. Analysis of One Turbulent Computation

In this section, we present the results obtained from the two simulations G_1 and G_2 on the large computational domain. The objective is to understand the mechanisms of interaction between vortices and turbulence and to obtain quantitative results about the aging process. These results will be compared with the laminar case (P_{lam}). For the analysis of the turbulence, the case without vortices (P_{thi}) is used as reference.

1. *Qualitative Description of the Phenomenon*

Figure 2 shows the evolution of the vortex pair in the case without axial velocity (G_1). In Figs. 2a–2d, one isosurface of the vorticity magnitude ($\Omega* = 0.06$) for different instants is drawn. The right vortex has a positive vorticity, and the left one has negative vorticity. At $t* = 0$ (Fig. 2a), the isosurfaces are rectilinear cylinders. In the surrounding turbulent field, no eddy with a vorticity magnitude as intense as $\Omega* = 0.06$ is present. The high levels of vorticity are concentrated inside the two vortices. For larger times, tubes with a vorticity greater than $\Omega* = 0.06$ appear. These structures roll around the vortices in the same direction as the swirling velocity of each vortex. The vorticity direction in these tubes is in the cross planes normal to the z axis, quite parallel to the azimuthal direction of the corresponding vortex, without preferential sense. Consequently, the axes of the vortices are no longer rectilinear. Their curvature seems to be more important in the direction joining the two vortices (x direction) and increases with the time. Similar structures have been evidenced by Melander and Hussain.[32] In their study of helical wave decomposition, they show the creation of polarized threads surrounding coherent structures. As in our case, these secondary structures spin azimuthally around the column vortex.

Figures 3a and 3b show two isosurfaces of axial velocity (z direction) and one isosurface of vorticity magnitude at the instants $t* = 0$ and 96, respectively. This latter isosurface $\Omega* = 0.15$ shows the location of the two wake vortices. The two isosurfaces of axial velocity correspond to the values $u_z* = \pm 0.035$ and 0.035, respectively. At $t* = 96$ some axial velocity sheets have appeared; they roll around the vortices. These structures, which do not exist at the beginning

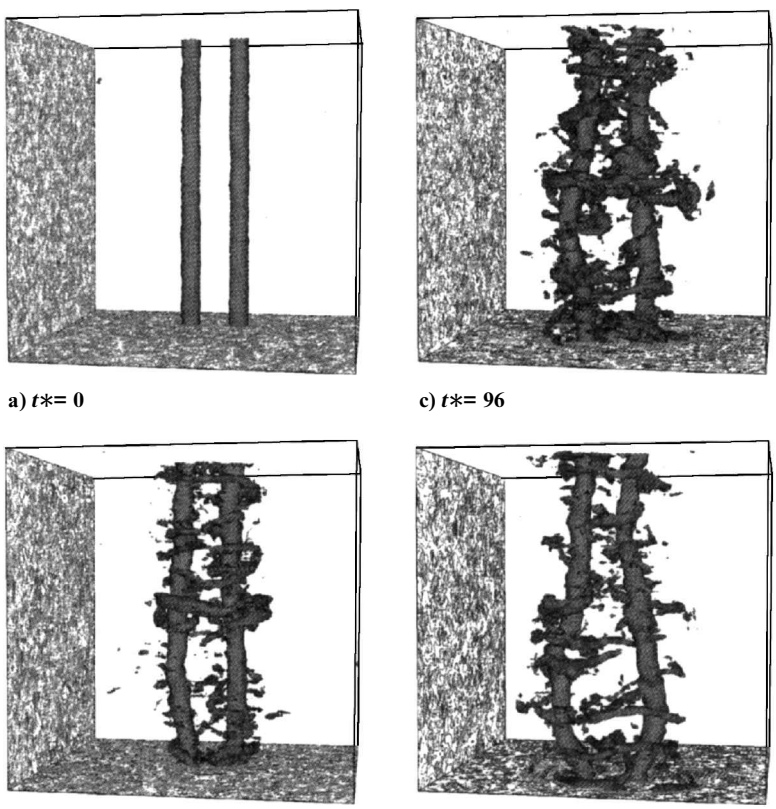

a) $t*= 0$ **c)** $t*= 96$

b) $t*= 48$ **d)** $t*= 144$

Fig. 2 Isosurface of vorticity magnitude.

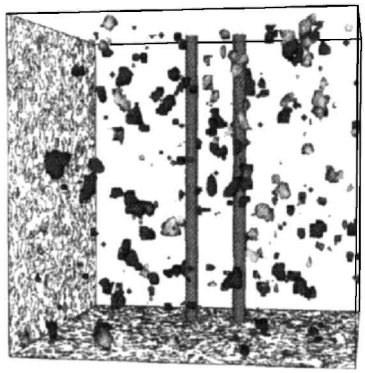

a) $t*= 0$

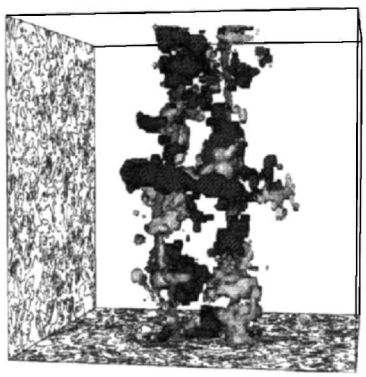

b) $t*= 96$

Fig. 3 Isosurface of axial velocity.

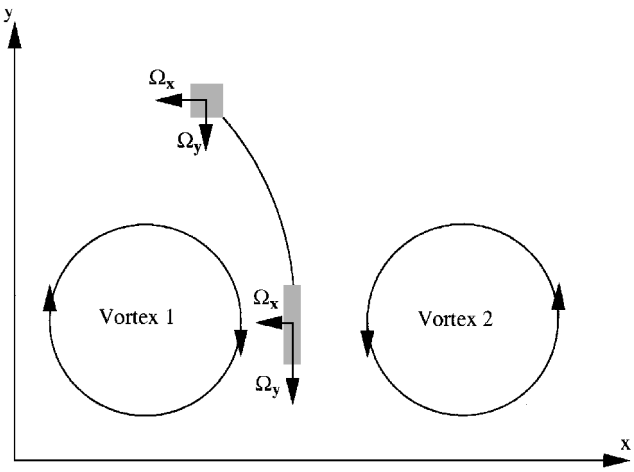

Fig. 4 Vortex stretching.

of the simulation, are created by the action of the vortices on the ambient turbulence. The phenomenon is antisymmetric: sheets of opposite sign alternate along the two vortices; their sign is directly related to the axis curvature of the related vortex. Later, these structures of axial velocity disappear.

2. Action of the Vortices on the Turbulence

To explain the mechanism involved in the process just described, let us consider a fluid element initially located above the vortices (Fig. 4). This element is entrained between the vortices by the mean flow they induced. The vorticity related to the vortices is localized in the near core region. Thus, as long as the fluid element is far from the vortices, all of the vorticity it contains is due to the turbulent eddies. Later, its evolution is driven by the equation of vorticity, which is in Cartesian coordinates (using the Einstein convention),

$$\frac{\mathrm{D}\Omega_i}{\mathrm{D}t} = \frac{\partial \Omega_i}{\partial t} + U_j \frac{\partial \Omega_i}{\partial x_j} = \Omega_j \frac{\partial U_i}{\partial x_j} + \nu \frac{\partial^2 \Omega_i}{\partial x_j \partial x^j} \qquad (13)$$

Table 2 Far and near zones definitions

	Near zone	Far zone
Mesh	$7 \times 32 \times 32$	$32 \times 32 \times 32$
Size	$2.1 \times 10.85 \times 10.85$	10.85^3
Limits relative to the pair center		
$x^*_{\min}, x^*_{\max}$	−1.05, 1.05	−5.25, 5.60
$y^*_{\min}, y^*_{\max}$	−5.25, 5.60	12.60, 23.45
$z^*_{\min}, z^*_{\max}$	−5.25, 5.60	−5.25, 5.60

Here, the main process is the vortex stretching mechanism expressed by the first term of the right-hand side of Eq. (13). The high value of the turbulence to vortices time scale ratio [Eq. (12)] implies that the turbulence is frozen on the time scale of the vortex evolution. For the velocity gradients $\partial U_i/\partial x_j$, the effect of turbulence is negligible, and only the mean velocity has to be taken into account. The velocity field induced by the vortices compresses the fluid element in the x direction and stretches it in the y direction. In consequence, the magnitude of the vorticity in the y direction Ω_y is increased; but the sign of Ω_y could be either positive or negative because it is given by the initial turbulent stochastic conditions. Concurrently, the magnitude of Ω_x tends to decrease. Then, after being moved between the vortices, the eddy does not leave the pair on a symmetric trajectory. Because of the global motion of the pair, it is entrained around one of the vortices, and azimuthal tubes are formed.

To check this interpretation, a comparative analysis of the turbulence properties in two different regions of the flow has been performed. The locations of these regions are defined relative to the vortex pair and move with them (see Table 2). The first one, referred to as the far zone, is sufficiently far away from the vortices to assume that the turbulence is free. The second one, referred to as the near zone, is situated between the two vortices but out of the core regions.

A way to investigate the action of the vortex stretching exerted by the vortex flowfield on the turbulence is to examine the evolution of the enstrophy in the neighborhood of the pair. For this reason we define the enstrophy tensor $\Phi_{ij} = \Omega_i \Omega_j$. To evaluate the total amount of enstrophy F, the classic scalar definition is used:

$$F = \frac{1}{2} \sum \Phi_{ii}$$

and to distinguish its distribution in each direction, the diagonal components Φ_{ii} are considered. The corresponding results for the case G_1 are presented in Fig. 5.

At $t* = 0$, all of the Φ_{ii} in the two zones are equal because all of the vorticity is due to the initial isotropic turbulence. In the far zone, the three components decrease regularly and continue to be equal to each other. This confirms that the ambient turbulence is a still isotropic decaying turbulence. In the near zone, the total strain induced by the vortex pair stretches the turbulent eddies and causes a rapid increase of the total amount of enstrophy. The maximum of F is reached near $t* = 70$. Afterward, the general decay of the ambient turbulence exceeds the enstrophy production by the stretching of the vortices, and F begins to diminish. The analysis of the diagonal components confirms the interpretation proposed before. Indeed, the augmentation of the enstrophy is mainly due to the increase of Φ_{yy}. A part of the increase of Φ_{xx} is caused by the fact that the stretching acts exactly in the y direction only for eddies located in the median plane between the two vortices. Thus a fraction of the enstrophy produced by the stretching is given to Φ_{xx}. Moreover, the mutual interactions of the turbulent eddies tend to redistribute energy between the different components of the fluctuations and lead to a spontaneous return to isotropy. This is the second cause for the increase of Φ_{xx} and the reason for the augmentation of Φ_{zz}. This redistribution goes on after Φ_{yy} has reached its maximum. In consequence, the maxima of Φ_{xx} and Φ_{zz} are reached later. From $t* = 140$, Φ_{xx} and Φ_{zz} have the same magnitude and then decrease rapidly. The G_2 simulation shows similar results: the axial velocity has no significant influence on that.

This strong production of vorticity in the plane normal to the z direction and the fact that the initial length scale L_e is greater than the vortex spacing d_0 explain the formation of alternated sheets of axial velocities. Indeed, when a turbulent eddy whose size is comparable to d_0 is stretched by the vortex induced velocity field, high axial

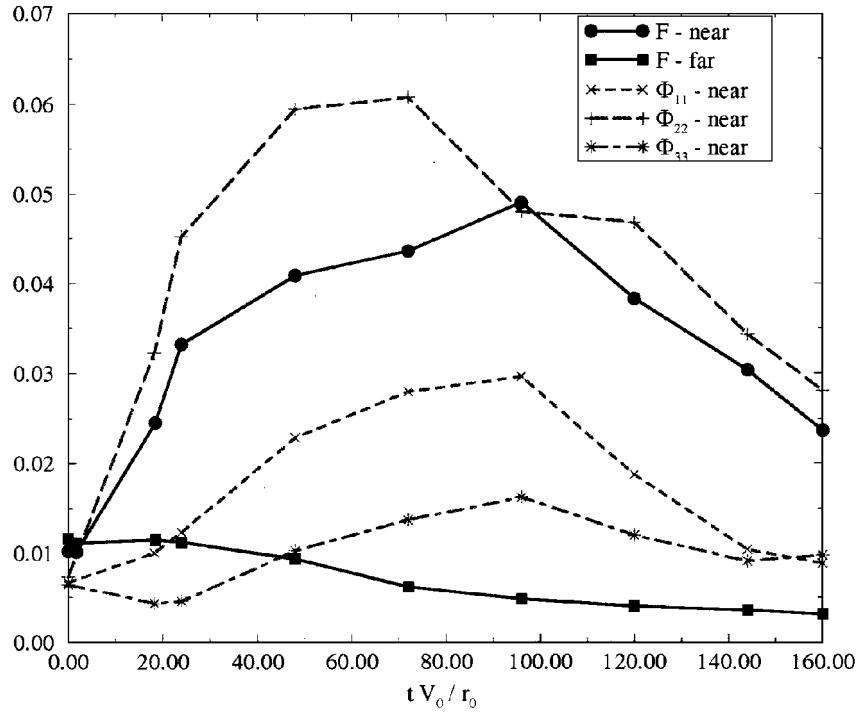

Fig. 5 Enstrophy vs time: case G_1.

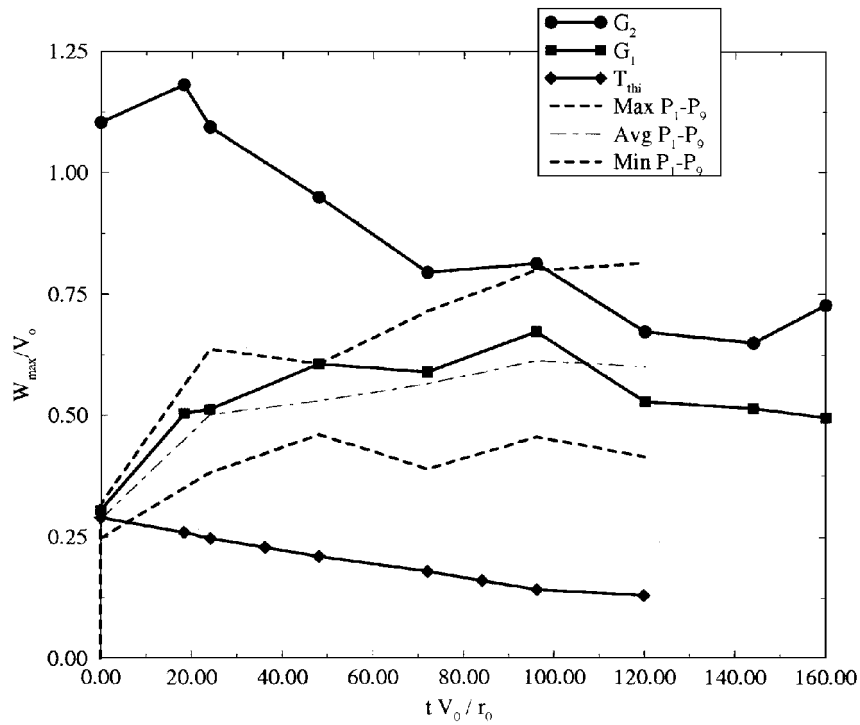

Fig. 6 Axial velocity vs time.

velocities are created near each vortex; their magnitude is close but their sign is opposite. After about $t* = 70$, the structures disappear due to the decay of the turbulence.

Figure 6 features the evolution of the maximal axial velocity over the whole flowfield. At $t* = 0$, for the cases of G_1 and P_{thi}, the only axial velocities are due to the turbulent fluctuations; their maximums, thus, have the same value of about $0.3V_0$. Then, the turbulent fluctuations of the case without vortices (P_{thi}) decrease continuously. At the opposite, in the case of G_1 the maximal axial velocity increases and reaches a maximum close to $0.7V_0$. The locations of these high axial velocities always remain close to the pair and follow it during its displacement. For the case of G_2, the initial maximal velocity is located at the vortex axis. Then, axial velocity in the core decreases because of the diffusion. From $t* = 100$, the maximal velocity created out of the core becomes predominant. Its magnitude is greater than for the case G_1 ($0.8V_0$) but its location is in the same region.

3. *Definitions of Parameters for the Vortex Description*

In this subsection, objective parameters for the description of the vortices are introduced. The goal is to perform a quantitative analysis of their evolution. For a complete characterization, different aspects have to be investigated, namely, the displacement, the deformation, and the decay. In the present situation, leaving aside the curvature of the vortex axis, which is an intrinsically three-dimensional phenomenon, the characteristic parameters of two-dimensional vortices can still be used for the description.

In what follows, the two vortices are distinguished by the subscripts $i = 1$ and 2. At a given instant t, the plane Cartesian coordinates $(x_{c,i}, y_{c,i})$ of the vortex center are determined by the

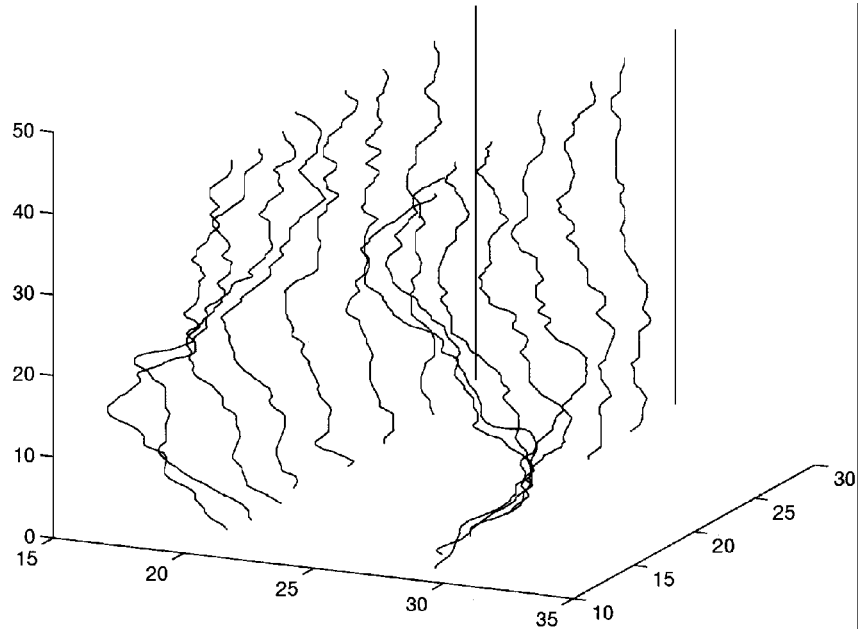

Fig. 7 Vortex centerlines: $t*= 0–160$; $\Delta t*= 24$, run G_1.

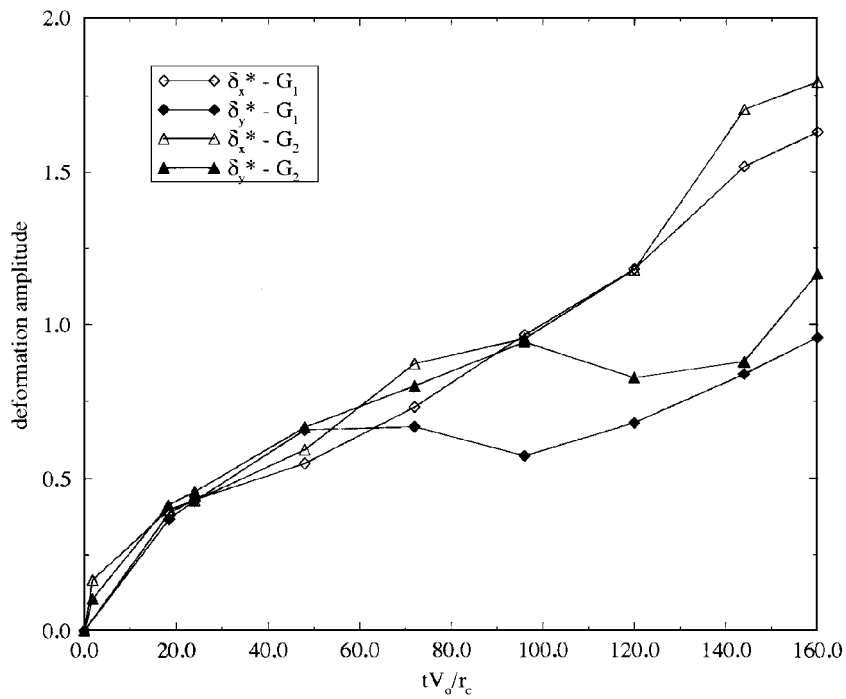

Fig. 8 Deformation magnitude vs time.

location of the pressure minimum in each cross plane $z = c^{ste}$. A line $[x_{c,i} = f_i(z), y_{c,i} = g_i(z)]$ is thus obtained (Fig. 7). Then, the position $(x_{t,i}, y_{t,i})$ of the equivalent two-dimensional vortex is defined by averaging in the z direction.

For the characterization of the decay, the core radius r_c and the maximal azimuthal velocity $V_{\max}$ have been chosen. Because of the presence of turbulent fluctuations, their values cannot be directly obtained from the velocity field in each cross plane. Thus, a two-dimensional flow is calculated by averaging the flow in all of the cross planes. But, before the averaging, the flowfield in each cross plane $z = c^{ste}$ is moved by a translation of vector $[-x_{c,i}(z), -y_{c,i}(z)]$. In this way, the effect of the deformation of the vortex axis is eliminated, and only the decay is taken into account. This operation is repeated independently for the two vortices; hence, two equivalent two-dimensional vortices are obtained. Finally, the values of r_c and $V_{\max}$ are determined by minimization of the mean squared difference between formula (1) summed for two vortices and the results of the simulation.

The main features of the vortex deformation can be obtained from the characteristics of the centerline $(x_{c,i}, y_{c,i})$. In the present work, attention is focused on the magnitude of the deformation, which can be analyzed from the standard deviation,

$$\delta_{x,i} = \left\{ \frac{1}{z_{\max}} \int_0^{z_{\max}} [x_{c,i}(z) - x_{t,i}]^2 \, dz \right\}^{\frac{1}{2}} \tag{14}$$

(for the y direction, a similar definition is used).

In Figs. 8–11, each plotted value is the average of the two vortices of the pair.

4. *Motion, Deformation, and Stability of a Vortex Pair*

As expected, the velocity induced by each vortex near its companion causes the whole motion of the pair in the positive y direction. The main effect of turbulence on this motion is to vary their spacing in the x direction: it has a direct consequence on the whole velocity. On the other hand, their spacing in the y direction seems not to be influenced by the turbulence.

The vortex deformations are illustrated in the Fig. 7. The centerlines of the vortices in the G_1 case are plotted for eight different

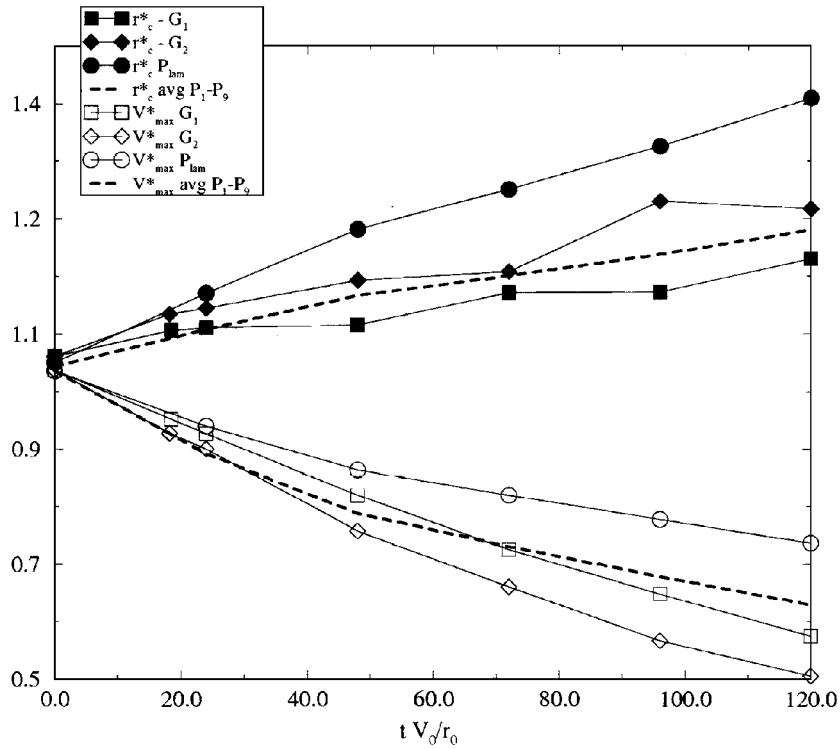

Fig. 9 Time evolution of r_c^* and V_{max}^*.

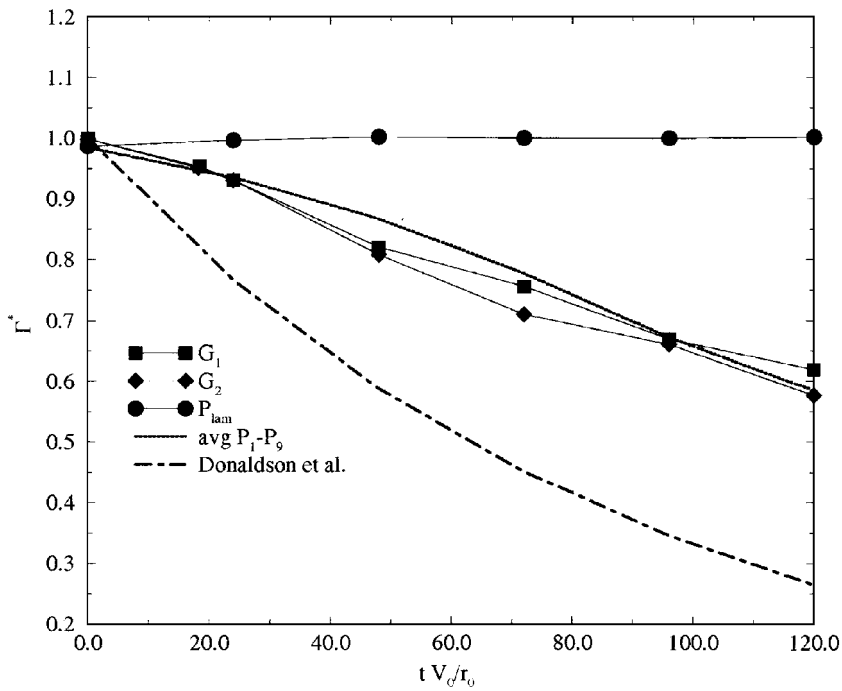

Fig. 10 Time evolution of the circulation Γ^*

instants with a regular time interval $\Delta t^* = 24$. In the initial condition the vortices are rectilinear. Then, perturbations appear. Short waves correspond to deformations in the x or in the y direction without preference. But the long-wave perturbation that appears corresponds only to deformations in the direction joining the vortices (x direction). The q-vortex G_2 case, not presented here, shows a similar behavior. The quantitative results about the deformation magnitudes are presented in Fig. 8. For $t^* \lesssim 70$, the deformations are about the same magnitude in the two directions and for the two cases. At $t^* = 70$, the standard deviations δ^* all range from 0.7 to 0.8. But for $t^* > 70$, the amplitude becomes larger in the x direction than in the y direction.

For $t^* \lesssim 70$, the deformations due to the random turbulent perturbations predominate. Thus, the deformation magnitudes are the same in all directions and their wavelengths are in the range of the turbulent eddies (from 1 to 10 d_0). After $t^* = 70$, the magnitude of the deformations is now essentially due to the long-wave perturbation, whose wavelength is equal to the domain size ($L^* = 46.9$). Its amplitude increases continuously up to the end of the simulation ($t^* = 160$), even though the turbulence decays. Hence, turbulence does not drive the vortex deformation anymore. The turbulence fluctuations have initiated an unstable antisymmetric deformation of the vortex, which is discussed in the work of Klein et al.[7] These authors have studied theoretically the interaction of nearly parallel filaments for perturbations whose wavelengths are long in comparison with the vortex spacing d_0. They show that for an antiparallel vortex pair, there is a finite-time collapse independent of the structure of the perturbation.[7] Here, the ratio of the length of the wave to the

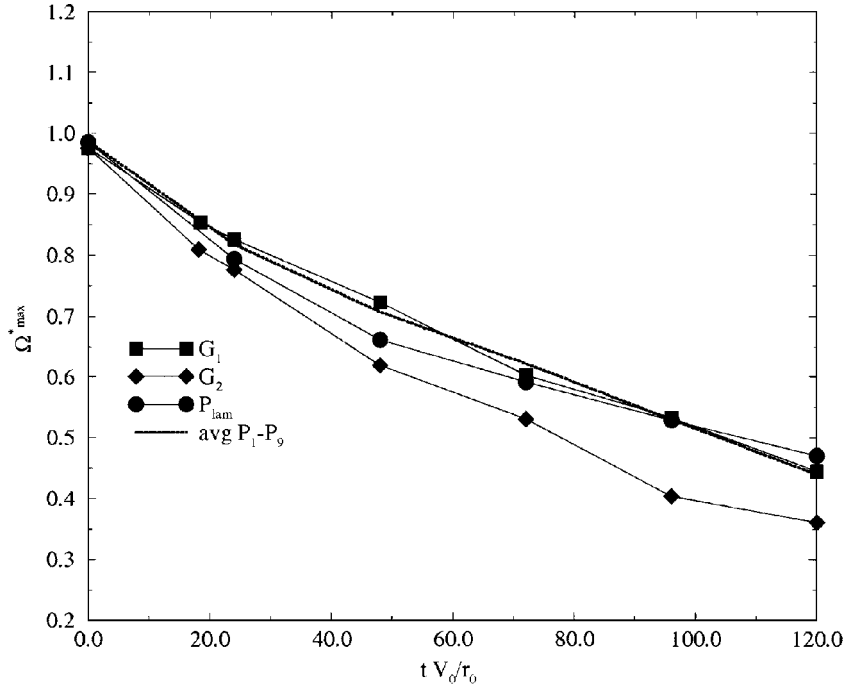

Fig. 11 Time evolution of the vorticity Ω^*_{max}.

vortex spacing is only about 2.9. Therefore, the theory does not rigorously apply but the mechanism is likely to be the same. Here, the waves developing have the maximal length allowed by the finite domain; thus, one cannot conclude that it is the most unstable one. The deformations observed here after $t* = 70$ suggest extending the unconditional instability of counter-rotating vortex pair in presence of turbulence and for finite length wave. Furthermore, the presence of axial velocity in the vortex cores seems to increase the growth rate of the instability.

5. *Aging of a Vortex Pair*

The effect of the aging process is analyzed from the radial distribution of the equivalent two-dimensional vortex defined earlier. The central region of the vortex ($0 \leq r* \leq 3$) is accurately approximated by the analytic expression of the Lamb–Oseen pair. In the outer region of the vortex, the fitting does not apply correctly: for a same core set of parameters (r_c and V_{max}) the decay with the distance is faster here than for the laminar solution of Lamb–Oseen. To improve the comparison between laminar and turbulent situations, Fig. 9 features the evolutions of the core radius r_c* and the maximal velocity V^*_{max} in the turbulent simulations (G_1, G_2) and in the laminar one (P_{lam}).

The G_1 case shows a stronger decay of the velocity V^*_{max} than the laminar case; this effect is reinforced in presence of axial core velocity (G_2). As expected, the ambient turbulence accelerates the aging process of the vortex. But the increase of the core radius r_c is slower in presence of turbulence. This must not be interpreted as a smaller diffusion of the vorticity because r_c does not correspond to a point of constant velocity magnitude, but to the point of maximal velocity. Thus, turbulence does not simply accelerate the laminar diffusion process as suggested from an approach based on an increase of the bulk viscosity. The mechanisms induced by turbulence are radically different. The use of the natural parameters r_c and V_{max} does not permit exhibiting its main characteristics. In consequence, we introduce now another representation based on another two parameters: a circulation Γ and a vorticity Ω_{max}.

For the Lamb–Oseen vortex [Eqs. (6) and (7)], the circulation at infinity is proportional to the product $r_c V_{max}$ and the maximal vorticity Ω_{max} in the vortex center is proportional to the ratio V_{max}/r_c. Here, we keep the same definitions for Γ and Ω_{max}. For a pair of vortices, the circulation far from a vortex is not characteristic of its own evolution. Furthermore, the fitting by the Lamb–Oseen expression is not valid far from the vortex. Thus, the parameters Γ and Ω_{max} are meaningful only for the properties of the vortex core: Γ is the global circulation and Ω_{max} the maximal intensity.

Figure 10 (and, respectively, Fig. 11) features the evolutions of Γ (and, respectively, Ω_{max}) in the two turbulent situations (G_1, G_2) and for the laminar reference (P_{lam}). We also added the model of Donaldson and Bilanin[13]:

$$\frac{d\Gamma}{dt} = -0.82\frac{u'\Gamma}{d_0} \tag{15}$$

In the laminar case, the circulation Γ remains constant (Fig. 10); each vortex behaves as if it was alone. That means that the two vortices are sufficiently far from each other to not interact. In the presence of turbulence, the circulation decreases; the axial velocity has no influence on this. On the other hand, the evolution of the maximal vorticity is similar in the laminar case and in the turbulent G_1 run; but the decay of the vorticity is faster in the presence of axial velocity (G_2).

The parameters Γ and Ω_{max} are related to two different mechanisms of the aging process. In the laminar situation, only one mechanism exists: the molecular diffusion. Hence, the evolution of the vortex is well represented by the maximal vorticity, which is proportional to the velocity gradient. But the action of turbulence should be decomposed in two parts. The first part is the turbulent transport of the vorticity, which can be roughly understood as an increase of the effective diffusion. Its magnitude is controlled by the velocity gradient as in the laminar case. Its effect is essentially to accelerate the laminar process by increasing the rate of decay of Ω_{max}. In the simulation presented here (G_1), the decay of the maximal vorticity is the same as in the laminar situation. The reason is that the spatial resolution of the simulation ($\Delta x* = 0.35$) is only about one-third of the initial core radius, and the length scale corresponding to the peak wave number in the initial dissipation spectrum ($2\pi/K_d = 3.97r_0$) is about four times the initial core radius. In consequence, the turbulent diffusion cannot act significantly on the scale of the core. The diffusion of the core vorticity is only due to molecular transport and the evolution of Ω_{max} is the same as in absence of turbulence. In the simulation G_2, the presence of the radial gradient of W causes a faster decay of Ω_{max}. In the laminar situation, the axial and radial diffusions are independent: the laminar decay of the q vortex and the Lamb–Oseen one is the same. But in the presence of turbulence the evolution of axial and radial velocity are coupled. Even without small-scale fluctuations able to induce turbulent diffusion of the vorticity, the presence of a gradient of axial velocity causes a faster decay of Ω_{max}.

The second mechanism involved in the action of the turbulence is related to the phenomenon described earlier: the vortex stretching process transfers vorticity from the vortex to the ambient turbulence.

This causes the decrease of the global intensity of the vortex and, thus, the circulation Γ decays. The vortex stretching is an inertial mechanism. It acts on all of the turbulent scales, but the major part of the enstrophy is given to the large scales, which are independent of the viscosity and can be significantly stretched before reaching the dissipative scales. This is very different from the diffusion process postulated by Donaldson and Bilanin.[13] Therefore, their model does not correctly predict the decay of the vortices.

B. Statistical Approach

The results just presented correspond to a unique run of the stochastic initial turbulence. To establish their sensitivity to the initialization, nine simulations (P_{1_9}) have been performed in a smaller domain ($L* = 28$); a grid of 81^3 nodes was used to conserve the same resolution. The only differences between these simulations are the random phases of the initial velocity fluctuations field in the spectral domain. This allows us to carry out statistics on the parameter characteristics of the vortices: probability density distribution, average values, and also extrema, which are fundamental for the hazard estimate.

First, let us go back to Fig. 6 to examine the dispersion of results around the maximal axial velocity. The averaged value obtained from the nine simulations is very close to those of the G_1 case. This means that the simulations G_1 and G_2, which have the same initial turbulence, are representative. Nevertheless, the difference between the two extrema becomes large and increases regularly with time. Considering the diverse runs, the axial velocity can go beyond $0.8V_0$ or remain fewer than $0.4V_0$. Therefore, the aircraft hazard related to the appearance of the horizontal vorticity tubes is very difficult to predict. The statistics of the vortex motion show that there is no general tendency for the vortices to go closer or farther from each other. Fluctuations in their spacing and in their global motion are controlled by the random turbulent fluctuations. When their spacing decreases, the pair accelerates in the y direction and vice versa. Also, it is noticeable that the laminar prediction (P_{lam}) is in the range of the turbulent results.

As already explained, the deformations of the vortex are driven by a long-wave instability. Therefore, the corresponding results depend on the domain size. Thus, no quantitative comparison can be made between the little domain simulations (P_{1_9}) and the large domain ones (G_1, G_2). Nevertheless, there is a large dispersion of the results of the nine simulations P_{1_9}: at $t* = 120$ the standard deviation of the deformations ranges from 0.5 to 3.

Regarding the aging process, the average values of the core radius r_c, the maximal velocity $V_{\max}$, the maximal vorticity $\Omega_{\max}$, and the circulation Γ are presented in Figs. 9–11. Opposite the motion and the deformation, the dispersion on the vortex characteristic is very weak. Consequently, the average values of all these parameters are very close to the results of the G_1 simulations. Therefore, a unique calculation is sufficient for determining their value.

C. Modeling

For the practical problem of the aircraft hazard caused by the wake vortices, simple models that can be used in real time in airports are needed. In this section, we use results obtained from the DNSs to help the design of such models.

The conclusions of this study seem to show that the aging process of the vortices is well described by the use of two parameters characteristic of classical two-dimensional vortices such as that of Lamb–Oseen. Among all of the possible couples, the choice of the maximal vorticity $\Omega_{\max}$ and the global core circulation Γ is particularly judicious because it permits us to separate the interaction between the vortices and the turbulence into two independent mechanisms. The evolution of Γ, which is related to the inertial vortex stretching process, involves essentially an interaction with the large turbulent scales (on the order of the vortex spacing d_0). The evolution of $\Omega_{\max}$ is related to the diffusion mechanisms, molecular or turbulent, and involves the small turbulent eddies (smaller than the core radius r_c).

Let us now take into account scale considerations. The whole problem, as formulated in this work, involves seven physical parameters: the initial characteristics of the pair (r_0, V_0, d_0), those of the turbulence (kinetic energy k, dissipation ϵ), the kinematic viscosity ν, and the time t. All of these quantities can be expressed using two independent units (length and time). Hence, the problem description required five independent dimensionless groups. Following the conclusion just recalled, we postulate that the evolutions of Γ and $\Omega_{\max}$ are driven by two independent mechanisms. The problem now is how to build the numbers relevant for these two processes.

For the vorticity, the mechanisms of diffusion have to be examined. In a laminar situation, the problem is entirely controlled by the Reynolds number: $Re = r_0 V_0/\nu$. In a turbulent situation, the turbulent diffusion of the core vorticity also has to be taken into account. It is proportional to the square of the characteristic velocity $u_l(r_0)$ of the eddies whose sizes are about those of the core radius. Assuming that the core radius is included in the inertial turbulent subrange, one finds $u_l(r_0) = (\epsilon r_0)^{1/3}$. Thus, we introduce another dimensionless number, the ratio between turbulent and molecular diffusion in the vortex core: $[(\epsilon r_0)^{2/3}]/(\nu V_0/r_0) = \epsilon^{2/3} r_0^{5/3}/\nu V_0$. Finally, we need to build a dimensionless time. For our presentation to be suitable for high-turbulence levels, we choose the turbulent scale: k/ϵ. Then, we propose the following expression for $\Omega_{\max}$:

$$\frac{\Omega_{\max}}{\Omega_0} = f\left(\frac{\Gamma_0}{\nu}, \frac{\epsilon^{\frac{2}{3}}\Gamma_0^{\frac{1}{3}}}{\nu\Omega_0^{\frac{4}{3}}}, \frac{\epsilon t}{k}\right) \tag{16}$$

In the case with an initial axial velocity W_0 in the vortex core, the gradient of $\Omega_w = W_0/r_0$ enhances the diffusion. The function f in Eq. (16) also depends then on the ratio of the two gradients: Ω_w/Ω_0.

The circulation Γ is controlled by the mutual stretching exerted between the vortices of the pair and the azimuthal turbulent eddies. This interaction occurs out of the core of the vortices. Actually, the eddies located between the vortices are those that are preferentially involved in the process. Thus, because d_0 is, in general, one order of magnitude larger than r_0, the vortex can be roughly considered as a filament only characterized by its circulation. If Γ_e is a characteristic circulation of the eddies in interaction with the wake vortex, and if l is a length scale representative of their spacing to the vortex, then l^2/Γ_e is the characteristic time scale of the action of the turbulence on the vortex. Reciprocally, l^2/Γ is the time scale of the action of the wake vortex on the turbulence. The ratio of these two time scales is the key parameter governing the evolution of Γ. For Γ_e, we can choose the product of the classical length scale $k^{3/2}/\epsilon$ by the root mean squared velocity $k^{1/2}$. This leads to the new number $r_0 V_0 \epsilon/k^2$. Actually, the eddies are essentially stretched in the region located between the two vortices of the pair. Thus, the ratio between the turbulent length scale $k^{3/2}/\epsilon$ and the vortex separation d_0 should be considered. This introduces the fifth and last dimensionless number required: $d_0\epsilon/k^{3/2}$. Therefore, the expression proposed for Γ is

$$\Gamma/\Gamma_0 = g(\epsilon\Gamma_0/k^2, \epsilon d_0/k^{\frac{3}{2}}, \epsilon t/k) \tag{17}$$

If the behavior of $\Omega_{\max}$ depends on the core circulation, the evolution of Γ is independent of the maximal vorticity. Fortunately, for the prediction of the hazard, the value of Γ is sufficient. Indeed, the maximal vorticity characterizes the structures of the flow inside the core although Γ represents the global intensity of the vortex.

Donaldson and Bilanin[13] first proposed a model for the decay of the circulation Γ of a vortex in the atmospheric turbulence. But they considered that the evolution of Γ was driven by the turbulent diffusion, as suggested in the more recent work of Zeman.[21] We have shown in this work that this is not correct. Therefore, we conclude with a warning: the prediction of the circulation is sufficient in practical problems, but it is necessary to relate it to the vortex stretching mechanism as is suggested in Eq. (17) and not to the properties of diffusion of the turbulence.

IV. Conclusion

The effect of an ambient homogeneous turbulence on the evolution of a vortex pair has been investigated from DNS.

The turbulence has a weak influence either on the motion or on the deformation of the pair. In the first stage, the large-scale turbulent fluctuations cause antisymmetric deformations of the vortex axes and initiate the known instability of antiparallel vortex pairs.[1] Then the deformations increase independently of the turbulence.

The main results concern the vortex aging process. By choosing a judicious set of parameters (the circulation Γ and the maximal vorticity $\Omega_{\max}$), the role of the large turbulent scales and that of the small ones can be separated into two independent mechanisms. This leads to a new formulation for vortex decay models. Namely, the circulation Γ, which is the principal parameter for hazard estimation, is found to depend on an inertial mechanism: the mutual stretching exerted between the wake vortices and the large turbulent structures. This contradicts all of the previous models, which postulate a diffusion mechanism.

Finally, the use of nine different turbulent runs allows us to prove that our conclusions are independent from the arbitrary turbulent initialization.

Acknowledgments

This work was supported by the Service Technique Navigation Aérienne under Research Grant STNA/95/110. The authors would like to thank the Commissariat à l'Energie Atomique Saclay and Centre National Universitaire Sud de Calcul for the access to their IBM SP2 and Meiko for their access to CS2.

References

[1]Crow, S., "Stability Theory for a Pair of Trailing Vortices," *AIAA Journal*, Vol. 8, No. 12, 1970, pp. 2172–2179.

[2]Crow, S., and Bate, E. J., "Lifespan of Trailing Vortices in a Turbulent Atmosphere," *Journal of Aircraft*, Vol. 13, No. 7, 1976, pp. 476–482.

[3]Sarpkaya, T., and Daly, J., "Effect of Ambient Turbulence on Trailing Vortices," *Journal of Aircraft*, Vol. 24, No. 6, 1987, pp. 399–404.

[4]Liu, H., "Tow-Tank Simulation of Vortex Wake Dynamics," *FAA Proceedings of the Aircraft Wake Vortices Conference*, edited by J. N. Hallock, Washington, DC, 1991, pp. 32-1, 32-26.

[5]Tombach, I., "Observations of Atmospheric Effects on Vortex Wake Behavior," *Journal of Aircraft*, Vol. 10, No. 11, 1973, pp. 641–647.

[6]Klein, R., and Majda, A., "An Asymptotic Theory for the Nonlinear Instability of Antiparallel Pairs of Vortex Filaments," *Physics of Fluids A*, Vol. 5, Feb. 1993, pp. 369–379.

[7]Klein, R., Majda, A., and Damodaran, K., "Simplified Equations for the Interaction of Nearly Parallel Vortex Filaments," *Journal of Fluid Mechanics*, Vol. 288, 1995, pp. 201–248.

[8]Rayleigh, J., "On the Dynamics of Revolving Fluids," *Proceedings of the Royal Society of London*, Series A, Vol. 93, 1916.

[9]Lessen, M., and Paillet, F., "The Stability of a Trailing Line Vortex. Part 2: Viscous Theory," *Journal of Fluid Mechanics*, Vol. 65, No. 4, 1974, p. 769.

[10]Ragab, S., and Sreedhar, M., "Numerical Simulation of Vortices with Axial Velocity Deficits," *Physics of Fluids A*, Vol. 7, March 1995, pp. 549–558.

[11]Virk, D., Hussain, F., and Kerr, R., "Compressible Vortex Reconnection," *Journal of Fluid Mechanics*, Vol. 304, 1995, pp. 47–86.

[12]Spalart, P., and Wray, A., "Initiation of the Crow Instability by Atmospheric Turbulence," *78th Fluid Dynamics Panel Symposium on the Characterization and Modification of Wakes from Lifting Vehicles in Fluids*, Vol. NATO–AGARD–CP-584 (Trondheim, Norway), AGARD, Paris, 1996, pp. 18-1, 18-8.

[13]Donaldson, C. D., and Bilanin, A., "Vortex Wakes of Conventional Aircraft," AGARDograph No. 204, May 1975.

[14]Bilanin, A., Teske, M., and Hirsh, J., "Neutral Atmospheric Effects on the Dissipation of Aircraft Vortex Wakes," *AIAA Journal*, Vol. 16, No. 9, 1978, pp. 956–961.

[15]Robins, R., and Delisi, D., "Numerical Study of Vertical Shear and Stratification Effects on the Evolution of a Vortex Pair," *AIAA Journal*, Vol. 28, No. 4, 1990, pp. 661–669.

[16]Zheng, Z., and Ash, R., "Prediction of Turbulent Wake Vortex Motion near the Ground," *Transitional and Turbulent Compressible Flows*, edited by J. N. Hallock, ASME FED Vol. 151, American Society of Mechanical Engineers, 1993, pp. 195–207.

[17]Squire, H., "The Growth of a Vortex in Turbulent Flow," *Aeronautical Quarterly*, Vol. 16, 1965, pp. 302–306.

[18]Owen, P., "The Decay of a Turbulent Trailing Vortex," *Aeronautical Quarterly*, Vol. 21, 1970, pp. 69–78.

[19]Iversen, J., "Correlation of Turbulent Trailing Vortex Decay Data," *Journal of Aircraft*, Vol. 13, No. 5, 1976, pp. 338–342.

[20]Phillips, W., "The Turbulent Trailing Vortex During Roll-up," *Journal of Fluid Mechanics*, Vol. 105, 1981, pp. 451–467.

[21]Zeman, O., "The Persistence of Trailing Vortices: A Modelling Study," *Physics of Fluids A*, Vol. 7, Jan. 1995, pp. 135–143.

[22]Risso, F., Corjon, A., and Stoessel, A., "Direct Numerical Simulation of Trailing Vortices in Homogeneous Turbulence," AIAA Paper 96-0802, Jan. 1996.

[23]Corjon, A., Risso, F., Stoessel, A., and Poinsot, T., "3D Direct Numerical Simulation of Wake Vortices: Atmospheric Turbulence Effects and Rebound with Crosswind," *78th Fluid Dynamics Panel Symposium on the Characterization and Modification of Wakes from Lifting Vehicles in Fluids*, Vol. NATO-AGARD-CP-584 (Trondheim, Norway), AGARD, Paris, 1996, pp. 28-1, 28-21.

[24]Stoessel, A., "An Efficient Tool for the Study of 3D Turbulent Combustion Phenomena on MPP Computers," *Proceedings of the High Performance Computing and Networking 95 Conference* (Milan, Italy), Springer–Verlag, Berlin, 1995, pp. 306–311.

[25]Lele, S. K., "Compact Finite Difference Schemes with Spectral-Like Resolution," *Journal of Computational Physics*, No. 103, 1992, pp. 16–42.

[26]Stoessel, A., and Baum, M., "Direct Numerical Simulation of 2D Turbulent Combustion Using Domain Decomposition Methods," SCS High Performance Computing 1994 Conf., La Jolla, CA, 1994.

[27]Lamb, H., *Hydrodynamics*, Dover, New York, 1932, p. 592.

[28]Batchelor, G., "Axial Flow in Trailing Line Vortices," *Journal of Fluid Mechanics*, Vol. 20, No. 4, 1964, pp. 645–658.

[29]Betz, A., "Verhaltern von WirbelSystemen," *ZAMM*, Vol. 12, No. 3, 1932, pp. 164–174.

[30]Mayer, E., and Powell, K., "Viscous and Inviscid Instabilities of a Trailing Vortex," *Journal of Fluid Mechanics*, Vol. 245, 1992.

[31]Hinze, J., *Turbulence*, McGraw–Hill, New York, 1959.

[32]Melander, M., and Hussain, F., "Polarized Vorticity Dynamics on a Vortex Column," *Physics of Fluids A*, Vol. 5, Aug. 1993, pp. 1992–2003.

A. Plotkin
Associate Editor